



# Study on the corrosion behavior of 316H stainless steel in molten NaCl–KCl–MgCl<sub>2</sub> salts with and without purification

Hua Ai<sup>1,2</sup> · Xin-Mei Yang<sup>1,2</sup> · Hua-Jian Liu<sup>1,2</sup> · Bing-Chuan Chen<sup>1,2</sup> · Ling Han<sup>1,2,3</sup> · Hua Sun<sup>1,2</sup> · Yan-Jun Chen<sup>1,2,3</sup> · Yuan Qian<sup>1,2</sup> · Jian-Qiang Wang<sup>1,2</sup>

Received: 21 April 2023 / Revised: 21 July 2023 / Accepted: 6 August 2023 / Published online: 7 December 2023

© The Author(s), under exclusive licence to China Science Publishing & Media Ltd. (Science Press), Shanghai Institute of Applied Physics, the Chinese Academy of Sciences, Chinese Nuclear Society 2023

## Abstract

The corrosion behavior of 316H stainless steel (SS) in the impure and purified NaCl–KCl–MgCl<sub>2</sub> salt was investigated at 700 °C. Results indicate that the main deleterious impurity induced corrosion in the impure salt was the absorbed moisture, present in the form of MgCl<sub>2</sub>·6H<sub>2</sub>O. 316H SS occurred severe intergranular corrosion with a corrosion depth of 130 μm for 1000 h in the impure NaCl–KCl–MgCl<sub>2</sub> salt. In contrast, the purification treatment of molten chloride salt by the dissolved Mg metal can remove the absorbed moisture, and the corresponding reactions were also discussed. As a result, the corrosiveness of NaCl–KCl–MgCl<sub>2</sub> salt is reduced significantly. 316H SS occurred slight uniform corrosion with a depth of less than 5 μm for 3000 h in the purified NaCl–KCl–MgCl<sub>2</sub> salt.

**Keywords** Stainless steel · Alloy · Chloride salt · Molten salt corrosion · High-temperature corrosion

## 1 Introduction

The sustainable growth of research interests in molten chloride salts are attributed to their superior physical and chemical properties; these salts act as heat transfer mediums and

coolants at elevated temperature [1, 2]. Currently, they have been utilized in molten chloride salt fast reactors (MCFRs) [1, 3, 4], concentrated solar power (CSP) plants [5–9], and hydrogen manufacturing equipment. Meanwhile, it poses a rigorous challenge due to the strong corrosiveness of molten chloride salts, resulting in the poor corrosion resistance of structural materials. Gregoire et al. [10, 11] verified that the corrosion rate of Inconel 600 in molten NaCl–KCl and NaCl–KCl–MgCl<sub>2</sub> was 10 and 5 mm/year, respectively. Vignarooban et al. [12] revealed a considerably greater corrosion rate of Hastelloy N alloy (> 150 μm/year) in NaCl–KCl–ZnCl<sub>2</sub> chloride salt than in LiF–NaF–KF fluoride salt. Ding et al. [13] evaluated the corrosion rates of 310 SS (1581 μm/year), Incoloy 800H (364 μm/year), and Hastelloy C276 (79 μm/year) in NaCl–KCl–MgCl<sub>2</sub> salt, pointing out that these alloys cannot meet the corrosion resistance requirements for commercial applications (< 30 μm/year) [9, 11, 14, 15]. Thus, the strong corrosiveness of molten chloride salts limits their widespread application in industrial fields.

The corrosion of chloride salts is attributed mainly to significant oxidizing impurities [16–19], such as moisture, oxygen, hydroxide ions, metallic ions, and acid radicals. Removing these impurities by the purification treatment effectively reduces the corrosiveness of molten chloride salts. After the

This work was supported by the National Science Foundation of Shanghai (No. 22ZR1474600), the National Natural Science Foundation of China (No. 12175302), the “Thorium Molten Salt Reactor Nuclear Energy System” Strategic Priority Research Program of the Chinese Academy of Sciences (No. XDA 02040000) and the “Transformational Technologies for Clean Energy and Demonstration,” Strategic Priority Research Program of the Chinese Academy of Sciences (No. XDA 21000000).

- ✉ Hua Ai  
aihua@sinap.ac.cn
- ✉ Xin-Mei Yang  
yangxinmei@sinap.ac.cn
- ✉ Yan-Jun Chen  
chenyanjun@sinap.ac.cn

- <sup>1</sup> Shanghai Institute of Applied Physics, Chinese Academy of Sciences, Shanghai 201800, China
- <sup>2</sup> Key Laboratory of Interfacial Physics and Technology, Chinese Academy of Science, Shanghai 201800, China
- <sup>3</sup> University of Chinese Academy of Sciences, Beijing 100049, China

purification treatment, the Fe-based alloys have been verified to possess excellent corrosion resistance at high temperatures [20, 21]. Thus, low-cost alloys have the potential to become structural materials for industrial applications. To date, researchers have attempted several techniques to purify molten salts [9, 22–24], such as:

- (1) Through the drying step upon heating the salt in an inert (Ar/N<sub>2</sub> gas) atmosphere.
- (2) By a chlorinating process with CCl<sub>4</sub>, HCl, or others.
- (3) By adding active Mg, Al, and Li metals into salts.
- (4) By vacuum distillation to remove oxygen-containing impurities from salt.

Adding reactive metals (such as Mg and Al) to chloride molten salt is the feasible method among these purification techniques. The Al powder could diffuse inward to the alloy substrate to form an aluminum-rich layer to reduce the corrosion of structural alloys [2]. However, adding Al would seriously affect the thermal-physics properties of the molten chloride salt. Ambrosek et al. [25] compared several purification methods (including Ar, Ar + CCl<sub>4</sub>, Ar + HCl, and Ar + Mg), and results showed that Mg was the preferable method to purify the MgCl<sub>2</sub>-based salts. The Mg addition could significantly affect the redox potential of molten chloride salts [26–28]. Raman and infrared spectra demonstrated that Mg treatment resulted in the formation of multiple complex chloride structures with low corrosiveness of molten salt [22]. Thus, the active Mg metal reduces molten salts' corrosiveness [29]. However, limited studies are comparing the corrosion behavior of iron-based alloys in purified and impure salts, and these results are important for the engineering application of chloride salts.

NaCl–KCl–MgCl<sub>2</sub> (33–21.6–45.4 mol.%) ternary eutectic salt is one of the most promising chloride salts with a relatively low melting point (385 °C) and a wide range of operating temperatures. 316H SS alloy is the candidate structural material for MCFR and CSP systems owing to its low cost and applicable mechanical properties at high temperatures [30, 31]. The approved usage temperature of 316H SS is up to 816 °C in ASME Section III, Subsection NH. The higher the molten salt temperature, the higher the energy conversion efficiency; simultaneously, the increased corrosiveness of molten chloride salts at higher temperatures results in severe corrosion damage to structural alloys [20]. The

molten NaCl–KCl–MgCl<sub>2</sub> salt should be purified to solve the rigorous corrosion and reduce its corrosiveness before use.

Considering the ideas above, the corrosion behavior of 316H SS alloy in the impure and purified salt was compared to evaluate the purification effect of Mg metal. The corrosion mechanism and corresponding reactions were discussed by analysis of molten salts and alloy samples.

## 2 Materials and methods

### 2.1 Materials

The test samples used in this work was 316H SS, which is a kind of Fe-based alloy composed of 17.31 wt% Cr, 13.04 wt% Ni, 2.56 wt% Mo, 1.98 wt% Mn, 0.4 wt% Si, and 0.06 wt% C. The bulk metal was cut into samples with a dimension of 15 mm × 10 mm × 5 mm by electrical discharge machining (EDM). Before corrosion tests, 316H samples were polished to 2000 grit sequentially with emery paper, then ultrasonically cleaned by deionized water and ethyl alcohol, respectively. All alloy samples were stored in the glove box, filled with high-purity Ar gas, when the preparations were completed.

The experimental ternary eutectic NaCl–KCl–MgCl<sub>2</sub> salt was composed of 33 mol% NaCl (99.5 wt% purity, analytical grade), 21.6 mol% KCl (99.5 wt% purity, analytical grade), and 45.4 mol% MgCl<sub>2</sub> (99.9 wt% purity, analytical grade). There were two types of NaCl–KCl–MgCl<sub>2</sub> salts. A portion of these component salts was mixed at room temperature, dried at 100 °C for 24 h in a stainless steel crucible, and named the impure NaCl–KCl–MgCl<sub>2</sub> salt. The other was mixed at room temperature in a stainless steel crucible and heated at 600 °C for 24 h by inserting a Mg metal rod into the salt in a glove box. During the heating process, some metallic Mg was dissolved into the liquid salt, and the concentration of the soluble Mg was measured to be approximately 250 ± 50 mg/Kg (~0.025 wt%). This concentration is far below the saturation solubility [26] of Mg metal in molten NaCl–KCl–MgCl<sub>2</sub> salt. This part was named as the purified NaCl–KCl–MgCl<sub>2</sub> salt. Before the corrosion experiments, the concentrations of major impurities in these two salts were analyzed by inductively coupled plasma optical emission spectrometer (ICP-OES) and shown in Table 1.

**Table 1** The major impurities in the impure and purified NaCl–KCl–MgCl<sub>2</sub> salts before corrosion by ICP-OES (unit: ppm by weight, mg/kg)

Metallic impurities	Fe	Cr	Ni	Mo
The impure NaCl–KCl–MgCl <sub>2</sub> salt	44.6 ± 3.7	2.1 ± 1.2	2.6 ± 0.3	1.5 ± 0.5
The purified NaCl–KCl–MgCl <sub>2</sub> salt	256 ± 15	10.5 ± 2.3	9.2 ± 2.2	2.1 ± 1.0

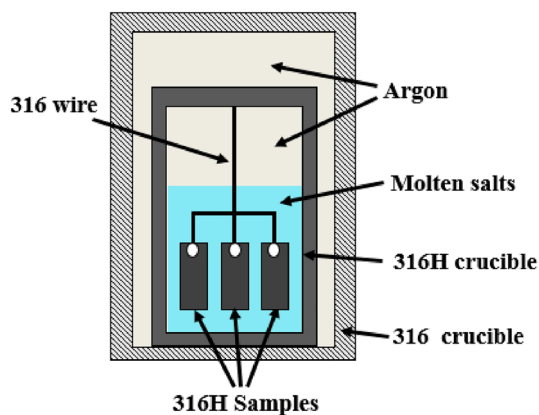


**Fig. 1** (Color online) The schematic diagram of the experimental setup for the corrosion test

## 2.2 Corrosion experiments and characterizations

Given that the service temperature of molten chloride salts is 500–700 °C [11, 22, 27], the experimental temperature for immersion corrosion tests is set at 700 °C in this study. The experimental setup consisted of two-layer crucibles in Fig. 1. The inner layer was a 316H SS crucible, which was the same material as the 316H SS samples to avoid dissimilar material interaction. The outer layer is the 316 SS crucible to ensure experimental safety. For each inner crucible, 200 g of the chloride salt (the impure or purified NaCl–KCl–MgCl<sub>2</sub> salt) was loaded with three pieces of parallel 316H SS samples to obtain the average corrosion data. Then, the outer crucible was welded and sealed to insulate it from air. All these preparations were conducted in the glove box. Then, the sealed crucibles were put in the heating furnace for different periods. The immersion times of 316H SS samples in the impure and purified NaCl–KCl–MgCl<sub>2</sub> salt were performed from 100 to 3000 h to investigate the microstructure evolution of corrosion.

After experiments, 316H SS samples were removed from the inner crucibles, cleaned with deionized water to remove residual solid salts, and dried in the air. The mass and dimension of each 316H SS sample were measured by an electronic balance and a Vernier caliper before and after corrosion. The weight change per area ( $\Delta m$ ) for each sample was obtained through Eq. 1.

$$\Delta m = (m_0 - m_1) / S \quad (1)$$

where  $m_0$  is the weight of a sample before corrosion, mg;  $m_1$  is the weight after corrosion, mg;  $S$  is the surface area of the sample before corrosion, cm<sup>2</sup>. After corrosion, the microstructure and elemental distribution of 316H SS samples were characterized using a scanning electron microscope (SEM, Carl Zeiss Merlin Compact) equipped with

an energy-dispersive X-ray spectrometer (EDS, Oxford Instruments X-Max). The X-ray diffraction (XRD: Bruker D8 Advance) analyzed the crystalline phases of the NaCl–KCl–MgCl<sub>2</sub> salt and 316H SS samples with a Cu K<sub>α1</sub> radiation source ( $\lambda = 1.5406 \text{ \AA}$ ) at 40 kV and 40 mA. The samples were scanned in a continuous  $\theta$ – $2\theta$  pattern in a range of  $10^\circ \leq 2\theta \leq 90^\circ$  in steps of  $0.02^\circ$  ( $2\theta$ ) and 0.15 s per step.

## 3 Results and discussion

### 3.1 Corrosion behavior of 316H SS in the impure NaCl–KCl–MgCl<sub>2</sub> salt

The major metallic impurities in the impure NaCl–KCl–MgCl<sub>2</sub> salt before corrosion were Fe: 45 mg/Kg, Cr: 2.1 mg/Kg, Ni: 2.6 mg/Kg, and Mo: 1.5 mg/Kg. The concentrations of metallic impurities were relatively low and could not drive the severe corrosion of 316H SS. Figure 2 shows the XRD patterns of the analytical grade NaCl, KCl, and MgCl<sub>2</sub> used in this work before corrosion. The characteristic peaks of pure species NaCl, KCl, and MgCl<sub>2</sub> phases are observed clearly in Fig. 2. Notably, the peaks corresponding to the MgCl<sub>2</sub>·6H<sub>2</sub>O were identified in the XRD pattern of MgCl<sub>2</sub>, suggesting that MgCl<sub>2</sub> could absorb H<sub>2</sub>O to form hydrated compounds MgCl<sub>2</sub>·xH<sub>2</sub>O ( $x=6$ ), which has been reported to be stable at room temperature [32].

Figure 3 presents the weight changes of 316H SS samples and the concentrations of metallic elements in the impure NaCl–KCl–MgCl<sub>2</sub> salt before and after corrosion. 316H SS samples underwent weight loss in the impure salt. The average weight changes per area were  $4.6 \pm 0.5$ ,  $8.7 \pm 1.0$ , and  $7.1 \pm 0.3 \text{ mg/cm}^2$  for 100, 500, and 1000 h, respectively. Fe, Cr, Ni, and Mo concentrations in the impure NaCl–KCl–MgCl<sub>2</sub> salt after corrosion remarkably increased

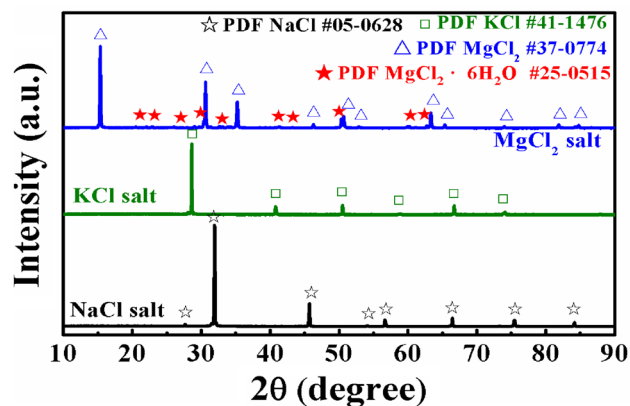


**Fig. 2** XRD patterns of the analytical grade NaCl, KCl, and MgCl<sub>2</sub> salt at room temperature

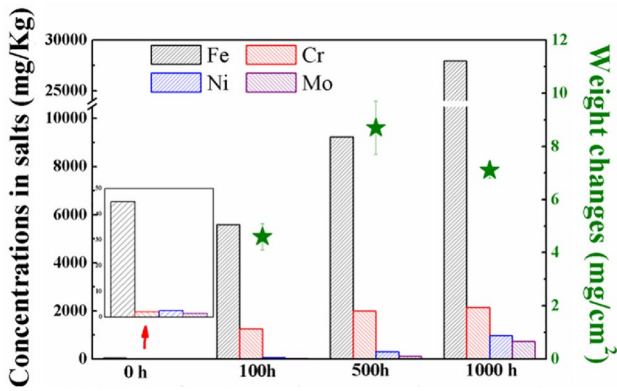
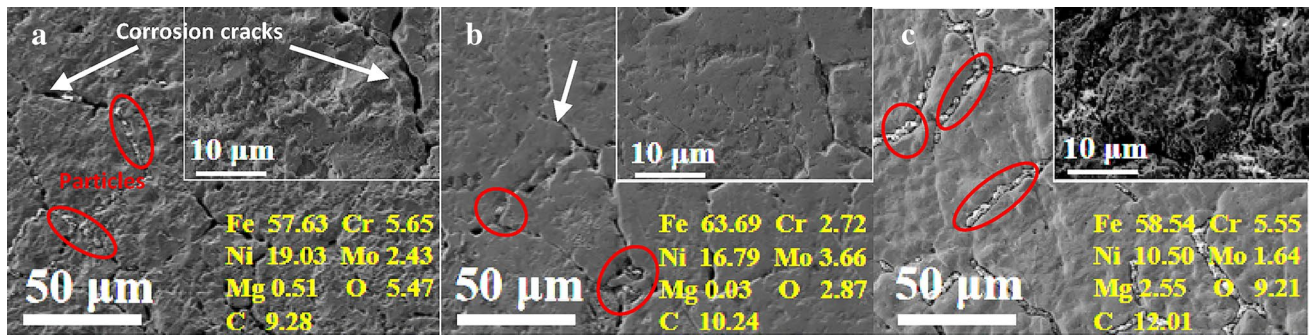


**Fig. 3** Weight changes per area of 316H SS samples and concentrations of dissolved alloying elements in the impure NaCl–KCl–MgCl<sub>2</sub> salt before and after corrosion

because of the dissolution of alloying elements from the alloy matrix into molten salts. After 100 h, the concentrations of elemental Fe and Cr dissolved in the salt increased from 45 to 5582 mg/kg and from 2 to 1265 mg/kg, respectively. After corrosion for 1000 h, Fe and Cr increased progressively to 27,961 and 2141 mg/kg, respectively. Meanwhile, the conventional noble elements Ni and Mo were also corroded, and the concentrations of Ni and Mo dissolved in the salt increased from 68 to 974 mg/kg and from 24 to

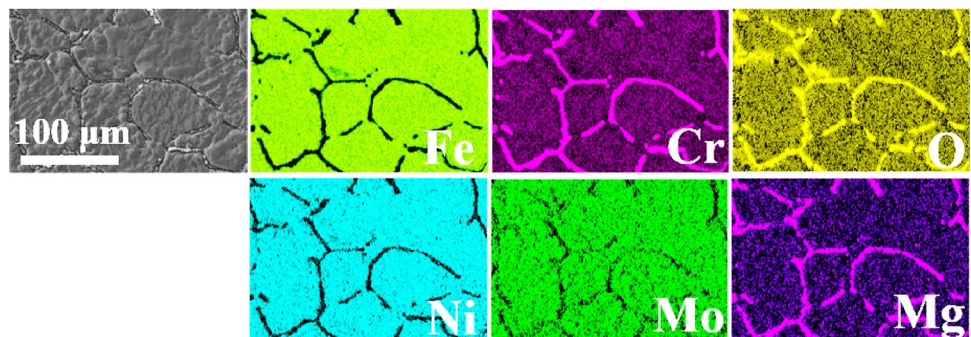
728 mg/kg when the time was increased from 100 to 1000 h, respectively. The significant decrease in the weight of 316H SS samples and the increased concentration of metallic elements in the molten salt indicate that 316H SS suffered severe corrosion damage in the impure NaCl–KCl–MgCl<sub>2</sub> salt at 700 °C.

Figure 4 shows the surface morphology of 316H SS samples corroded in the impure NaCl–KCl–MgCl<sub>2</sub> salt at 700 °C for 100–1000 h. The 316H SS exhibited significant intergranular corrosion, with the alloy surface relatively rough and grain boundaries increasingly looser. EDS results showed that the contents of Cr, Fe, Ni, and Mo in the alloy surface were notably reduced compared to the original composition of 316H SS, indicating the outward diffusion of these elements from the alloy matrix to molten salts during the corrosion process. Some oval particles were deposited in the grain boundaries and marked by red lines. Combining with the EDS mappings in Fig. 5, it can be assumed that these particles were relatively enriched in elements Cr, Mg, and O and poor in Fe, Ni, and Mo. Figure 6 is the XRD pattern of 316H SS samples before and after corrosion in the impure NaCl–KCl–MgCl<sub>2</sub> salt. The characteristic peaks of (111), (200), and (220) of austenite structure in the 316H SS were retained largely after corrosion. The new peaks in the XRD patterns of 316H SS after corrosion corresponded to the phase of MgCr<sub>2</sub>O<sub>4</sub>. It was deduced that the deposited



**Fig. 4** (Color online) Surface SEM images and the content (in weights, wt%) of major elements in the surface of 316H SS after corrosion in the impure NaCl–KCl–MgCl<sub>2</sub> salt at 700 °C for **a** 100 h, **b** 500 h, and **c** 1000 h

**Fig. 5** (Color online) SEM images and EDS mappings of elements in the 316H SS surface exposed in the impure NaCl–KCl–MgCl<sub>2</sub> salt for 1000 h



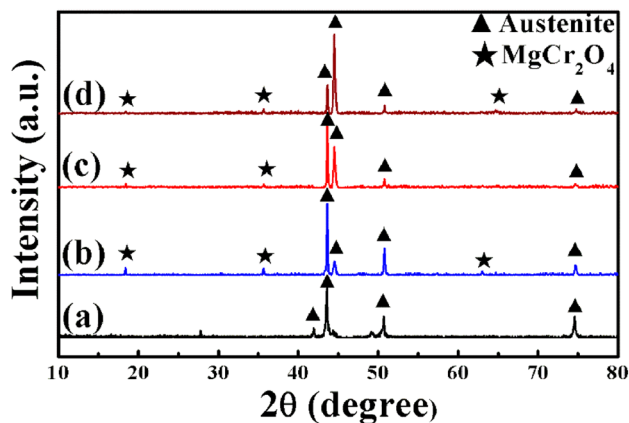


**Fig. 6** XRD patterns of 316H SS samples **a** before corrosion and after corrosion in the impure NaCl–KCl–MgCl<sub>2</sub> salt at 700 °C for **b** 100 h, **c** 500 h, and **d** 1000 h

precipitates enriched in Cr, Mg, and O elements in the grain boundaries should be MgCr<sub>2</sub>O<sub>4</sub>, consistent with the previous report [10, 33].

The cross-sectional SEM images in Fig. 7 reveal that all 316H SS samples underwent severe intergranular corrosion in the impure NaCl–KCl–MgCl<sub>2</sub> salt. Numerous corrosion voids were distributed along the grain boundaries. The corrosion depth of 316H SS samples was approximately 90, 120, and 130 μm for 100, 500, and 1000 h, respectively. The EDS mappings (Fig. 8) demonstrate that the depletion of Cr, Fe, Ni, and Mo of 316H SS samples was mainly along the grain boundaries. The Cr-depletion layer in the cross section was ~100 μm after corrosion for 100 h, slightly higher than the depth of intergranular corrosion voids (90 μm).

**Fig. 7** (Color online) The cross-sectional SEM images of 316H SS samples after corrosion in the impure NaCl–KCl–MgCl<sub>2</sub> salts at 700 °C for **a** 100 h, **b** 500 h, and **c** 1000 h

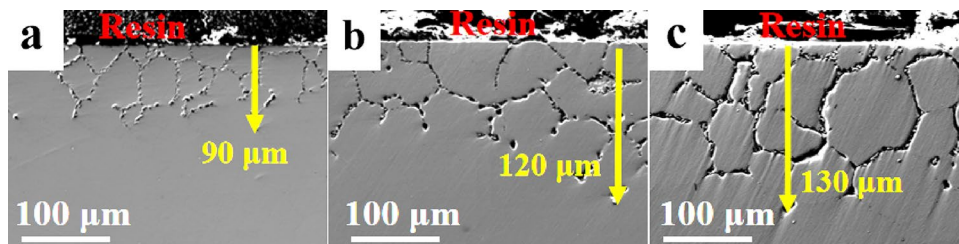
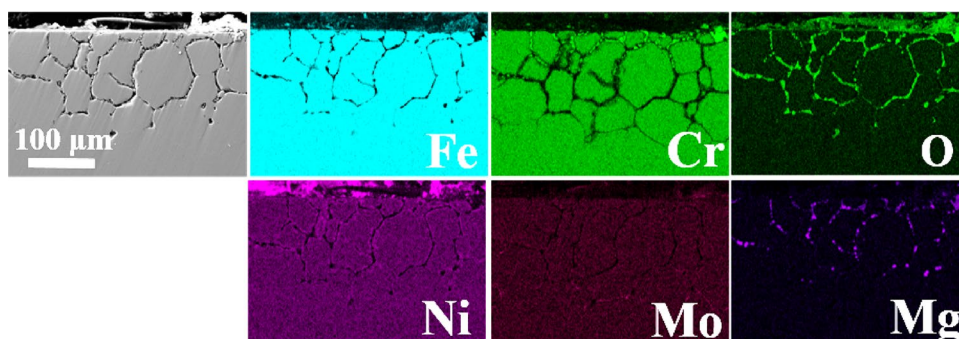


**Fig. 8** (Color online) Cross-sectional SEM images and EDS mappings of alloying elements in the 316H SS sample after corrosion in the impure NaCl–KCl–MgCl<sub>2</sub> salt at 700 °C for 1000 h



Considering corrosion voids resulted from clustering vacancies, formed by the continuous depletion of alloying elements. Thus, the thickness of the Cr-depletion layer was thicker than that of corrosion voids.

Meanwhile, some precipitates enriched in Cr, Mg, and O were observed in the near-surface region, mainly attributed to the formation of MgCr<sub>2</sub>O<sub>4</sub>, confirmed by XRD and EDS results. Within the region of corrosion voids, some particles enriched in elements Mg and O were distributed along grain boundaries, which resulted from the deposition of MgO during the corrosion process. The above results indicate that 316H SS had poor corrosion resistance and exhibited intergranular corrosion in the impure NaCl–KCl–MgCl<sub>2</sub> salt; the degree of intergranular corrosion was increased with increasing time. It is shown that the impure NaCl–KCl–MgCl<sub>2</sub> salt was highly corrosive and caused extreme corrosion damage to 316H SS. Therefore, the NaCl–KCl–MgCl<sub>2</sub> salt without purification is not suitable for engineering applications.

### 3.2 Corrosion behavior of 316H SS in the purified NaCl–KCl–MgCl<sub>2</sub> salt

The results in Sect. 3.1 indicate that the strong corrosiveness of the impure NaCl–KCl–MgCl<sub>2</sub> salt hinders its engineering application. Therefore, Mg metal was applied to purify the molten chloride salt. Then, the corrosion behavior of 316H SS in the purified NaCl–KCl–MgCl<sub>2</sub> salt was investigated to evaluate the effectiveness of the purification treatment.

The weight changes of 316H SS samples and concentrations of metallic elements after corrosion in the purified NaCl–KCl–MgCl<sub>2</sub> salt are shown in Fig. 9, where the minus sign (–) indicates an increase in weight after corrosion. The

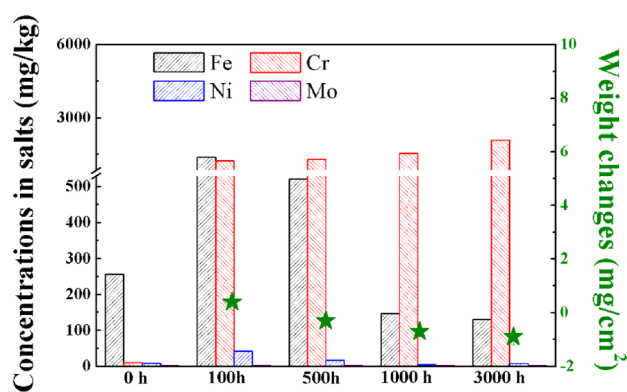


**Fig. 9** Weight changes per area of 316H SS samples and concentrations of dissolved alloying elements in the purified NaCl–KCl–MgCl<sub>2</sub> salt before and after corrosion

average weight changes of 316H SS samples were  $0.4 \pm 0.1$ ,  $-0.3 \pm 0.2$ ,  $-0.7 \pm 0.2$ , and  $-0.9 \pm 0.3$  mg/cm<sup>2</sup> for 100, 500, 1000, and 3000 h corrosion, respectively. By comparison, the weight variation of 316H SS samples in the purified NaCl–KCl–MgCl<sub>2</sub> salt was much smaller than that obtained in the impure salt. For 100 h immersion, the weight changes in the purified salt ( $0.4 \pm 0.1$  mg/cm<sup>2</sup>) was approximately one-tenth of that in the impure NaCl–KCl–MgCl<sub>2</sub> salt ( $4.6 \pm 0.5$  mg/cm<sup>2</sup>), indicating the Mg treatment could effectively mitigate the corrosion degree of 316H SS. Moreover, the weight gain of 316H SS samples was observed after corrosion from 500 to 3000 h, which was different from the severe weight loss in the impure NaCl–KCl–MgCl<sub>2</sub> salt. Given that the dissolution of alloying elements results in weight loss, and the deposition of corrosion products may lead to an increase in weight, it is deduced that the corrosion mechanism of 316H SS in the purified salt has been changed when compared to impure NaCl–KCl–MgCl<sub>2</sub> salt.

Fe, Cr, Ni, and Mo concentrations in the purified NaCl–KCl–MgCl<sub>2</sub> salt before corrosion were 256, 10, 9, and 2 mg/kg, respectively. The high concentration of Fe was derived mainly from the stainless steel crucible, which was used to prepare the purified salt during the heating process with a Mg rod. After corrosion for 100 h, Fe, Cr, and Ni increased to 1378, 1242, and 42 mg/kg. Then, Cr was increased continually to 2090 mg/kg for 3000 h corrosion, but Fe and Ni decreased slightly with time, and the concentration of Mo in the salt remained almost unchanged. Speculatively, the corrosion of 316H SS in the purified salt was mainly dominated by the dissolution of the active Cr element, and Mg treatment distinctly alleviated the corrosion rate of 316H SS in molten NaCl–KCl–MgCl<sub>2</sub> salt.

Figure 10 shows the surface morphology of 316H SS corroded in the purified NaCl–KCl–MgCl<sub>2</sub> salt. The relatively smooth surface of the corroded samples indicated that 316H SS underwent a slight corrosion attack at 700 °C for

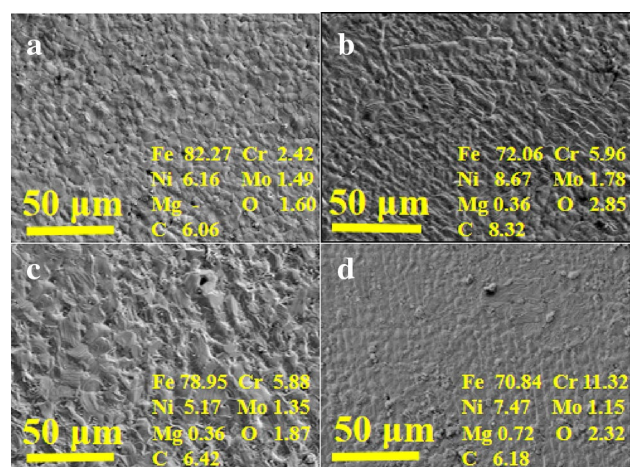


**Fig. 10** Surface SEM images of 316H SS and the contents of major elements (in weights, wt%) after corrosion in the purified NaCl–KCl–MgCl<sub>2</sub> salt at 700 °C for **a** 100 h, **b** 500 h, **c** 1000 h, and **d** 3000 h

100–3000 h immersion. The Cr content on the alloy surface decreased, and the Fe content increased compared to the composition of the 316H SS matrix. This phenomenon was attributed to the depletion of Cr from the alloy and the accumulation of Fe on the alloy surface during the corrosion process. The cross-sectional SEM images (Fig. 11) also demonstrate that 316H SS suffered minor corrosion with a maximum corrosion depth of approximately 3 μm in the purified NaCl–KCl–MgCl<sub>2</sub> salt. Figure 12 presents EDS mappings of 316H SS after corrosion for 1000 h and 3000 h. The obvious depletion of Cr and the evident enrichment of Fe were observed through the distribution of alloying elements, which was consistent with the results in Fig. 10. Therefore, the reaction between Fe ions in molten salt (256 mg/Kg) and the Cr atoms in the alloy surface can be simplified as  $x\text{Cr} + y\text{FeCl}_x = y\text{Fe} + x\text{CrCl}_y$  ( $x, y = 2/3$ ), resulting in the accumulation of Fe atoms and the depletion of Cr atoms in the corroded surface. A layer of corrosion products with a depth of 2 μm (Fig. 11d) was observed on the alloy surface for 3000 h corrosion, which was confirmed to be MgO (Fig. 12b) and has been reported by Ding [27] and Gregoire [11]. Due to the low solubility in molten chloride salt, MgO would precipitate from the salt to form a continuous oxide layer. The relatively dense MgO layer could protect the alloy bulk against further corrosion from the molten salt.

To assess the extent of the corrosion attack, the line-scan mode in EDS measured the maximum Cr-depleted thickness, and the thickness of the Cr depletion layer with the corrosion duration is summarized in Fig. 13. The results showed that a rapid increase of the Cr-depleted layer in the early stage, and then a slow increase to a steady state in the stable corrosion period. In Fig. 13, the maximum Cr-depleted layer was about 5 μm for 3000 h, and

**Fig. 11** Cross-sectional SEM images of 316H SS samples corroded in the purified NaCl–KCl–MgCl<sub>2</sub> salt at 700 °C for **a** 100 h, **b** 500 h, **c** 1000 h, and **d** 3000 h

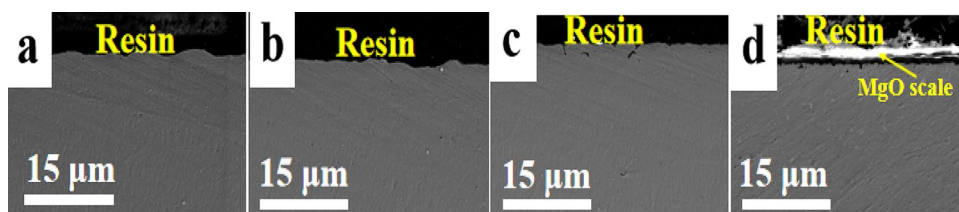


**Fig. 12** (Color online) Cross-sectional SEM–EDS mappings of 316H SS samples after corrosion in the purified NaCl–KCl–MgCl<sub>2</sub> salt at 700 °C for **a** 1000 h and **b** 3000 h

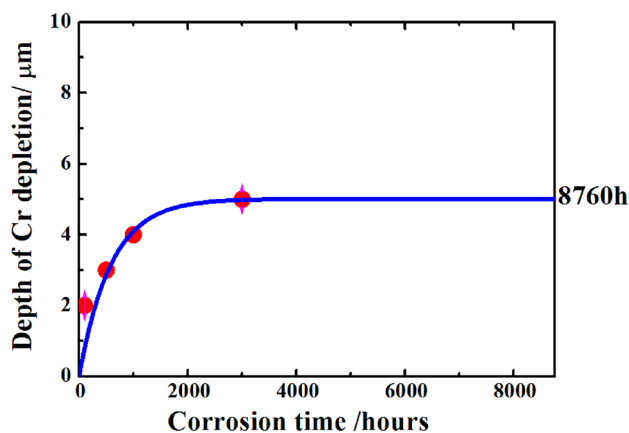
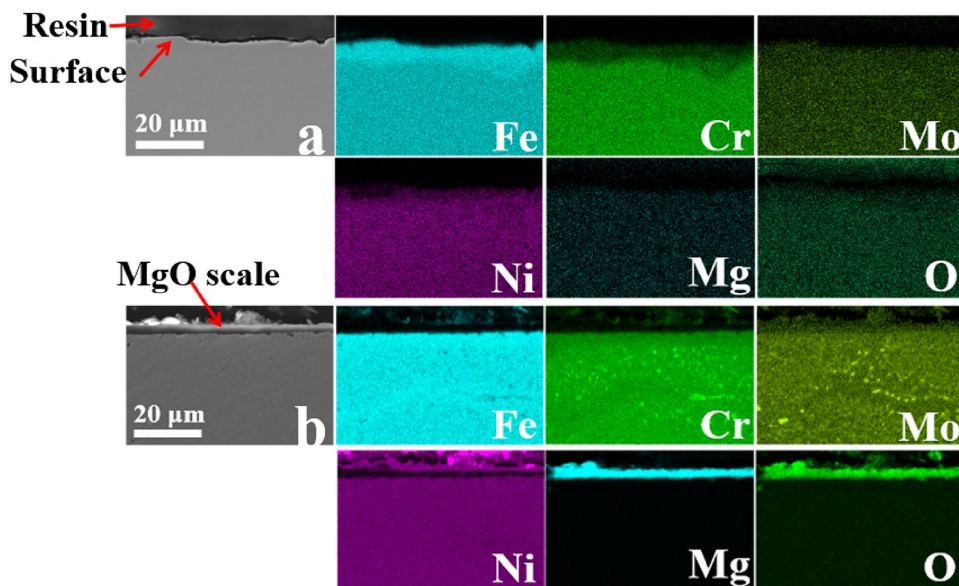


**Fig. 13** The thickness of the Cr depletion layer of 316H SS after corrosion for different exposing durations in the purified NaCl–KCl–MgCl<sub>2</sub> salt at 700 °C

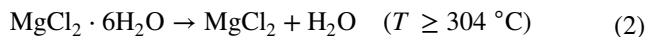
extrapolation indicated that the corrosion rate of 316H SS was less than 10 μm/year in the purified NaCl–KCl–MgCl<sub>2</sub> salt. The above experimental results show that the purification of the molten chloride salt through the Mg metal could significantly reduce its corrosiveness, and 316H SS exhibited excellent corrosion resistance in the purified NaCl–KCl–MgCl<sub>2</sub> salt.

## 4 Discussion

The above experimental results reveal that 316H SS suffered severe intergranular corrosion in the impure NaCl–KCl–MgCl<sub>2</sub> salt. The corrosiveness of the salt was significantly inhibited when purified by Mg metal. Interestingly, the concentration of metallic elements in the purified NaCl–KCl–MgCl<sub>2</sub> salt was considerably higher than in the impure salt (Table 1). In contrast, the corrosiveness of the impure salt was much stronger than the purified salt. It was deduced that the corrosiveness of metallic impurities in molten salts is relatively weak, and the corrosion effects of metallic impurities are negligible. The role of Mg metal during the purification treatment was elaborated to clarify the corrosion behavior of 316H SS in molten chloride salt.

The analytical grade NaCl, KCl, and MgCl<sub>2</sub> salts were employed to prepare the ternary eutectic salt. For the impure NaCl–KCl–MgCl<sub>2</sub> salt, these analytical salts were mixed in the air atmosphere and dried at 100 °C for 24 h. The hygroscopic MgCl<sub>2</sub> absorbed moisture from the air to form hydrated compounds MgCl<sub>2</sub>·6H<sub>2</sub>O, which XRD is verified in Fig. 2. The corrosion tests were conducted at 700 °C, MgCl<sub>2</sub>·6H<sub>2</sub>O occurred the hydrolysis reaction,

and decomposed to H<sub>2</sub>O, HCl, and MgO, above 304 and 415 °C during the heating process through Eqs. 2 and 3 [11, 32]. As strong oxidizing impurities, H<sub>2</sub>O and HCl both drive the corrosion of structural alloys through possible reactions shown in Table 2 [34]. Gibbs free energies show that reactions among H<sub>2</sub>O, MgCl<sub>2</sub>, HCl, and major alloying elements can drive the dissolution of Fe/Cr atoms to form corresponding metal ions, resulting in the evident weight loss of 316H SS. The depletion of alloying elements was preferentially outwardly diffused along grain boundaries, resulting in the severe intergranular corrosion of 316H SS. Reactions among CrCl<sub>x</sub> (x = 2, 3), H<sub>2</sub>O, and Ni/Mo can drive the corrosion of Ni/Mo to form NiCl<sub>2</sub>/MoCl<sub>3</sub>, leading to the increased concentration of Ni and Mo in salts (Fig. 3), although both Ni and Mo are noble elements. During the pyrohydrolysis process, the generated O<sup>2-</sup> would react with Cr atoms to produce Cr<sub>2</sub>O<sub>3</sub> owing to the strong affinity between Cr<sup>3+</sup> and O<sup>2-</sup> ions. The formed MgO in Table 2 was mainly deposited on the alloy surface and then diffused into the corrosion voids due to its small solubility in the molten chlorides [9, 10]. Besides, MgO could further react with Cr<sub>2</sub>O<sub>3</sub> to form MgCr<sub>2</sub>O<sub>4</sub>, confirmed by XRD and EDS results, mainly distributed along grain boundaries.



When the impure NaCl–KCl–MgCl<sub>2</sub> salt was purified by Mg metal at 600 °C for 24 h, some Mg atoms were dissolved

into the molten chloride salt with a concentration of about 250 ± 50 mg/Kg (~0.025 wt%). Possible reactions in Table 3 show that Mg metal can react with oxidizing impurities, such as H<sub>2</sub>O, HCl, and metallic ions, to reduce their concentrations in molten chloride salts. These hazardous impurities have been pre-reacted with the dissolved Mg to form MgO and H<sub>2</sub>. Theoretically, the reactivity of active Mg metal with impurities was greater than that of alloying element with impurities because the electromotive force (EMF) of Mg<sup>2+</sup>/Mg (–2.646 V vs. Pt) was more negative than that of Cr<sup>3+</sup>/Cr (–1.181 V vs. Pt) and Fe<sup>3+</sup>/Fe (–0.852 V vs. Pt) in NaCl–KCl–MgCl<sub>2</sub> eutectic salt [35]. When corrosion experiments were conducted at 700 °C, oxidizing impurities could preferentially react with the dissolved Mg metal rather than alloying elements (Cr/Fe) in the 316H SS; Mg metal acted as the corrosion inhibitor to lower the

**Table 3** Possible reactions between Mg and impurities during the purification process in NaCl–KCl–MgCl<sub>2</sub> salt at 600 °C and the corresponding Gibbs free energies

Reactions	ΔG at 600 °C (KJ/mol)
Mg + 2 HCl (g) = MgCl <sub>2</sub> + H <sub>2</sub> (g)	–304.493 ✓
Mg + H <sub>2</sub> O(g) = MgO + H <sub>2</sub> (g)	–308.020 ✓
Mg + FeCl <sub>2</sub> = MgCl <sub>2</sub> + Fe	–272.721 ✓
1.5 Mg + FeCl <sub>3</sub> = 1.5 MgCl <sub>2</sub> + Fe	–516.690 ✓
Mg + CrCl <sub>2</sub> = MgCl <sub>2</sub> + Cr	–217.506 ✓
1.5 Mg + CrCl <sub>3</sub> = 1.5 MgCl <sub>2</sub> + Cr	–383.181 ✓
Mg + NiCl <sub>2</sub> = MgCl <sub>2</sub> + Ni	–330.567 ✓
2.5 Mg + MoCl <sub>5</sub> = Mo + 2.5 MgCl <sub>2</sub>	–1001.645 ✓

**Table 2** Possible reactions and the corresponding standard Gibbs free energies at 700 °C during the corrosion process of 316H SS in the impure NaCl–KCl–MgCl<sub>2</sub> salt

Reactions	ΔG at 700 °C (KJ/mol)
MgCl <sub>2</sub> + H <sub>2</sub> O (g) + Fe = MgO + FeCl <sub>2</sub> + H <sub>2</sub> (g)	–34.535 ✓
1.5MgCl <sub>2</sub> + 1.5H <sub>2</sub> O (g) + Fe = 1.5MgO + FeCl <sub>3</sub> + 1.5H <sub>2</sub> (g)	50.860
2HCl (g) + Fe = FeCl <sub>2</sub> + H <sub>2</sub> (g)	–19.871 ✓
6HCl (g) + 2Fe = 2FeCl <sub>3</sub> + 3H <sub>2</sub> (g)	72.856
MgCl <sub>2</sub> + H <sub>2</sub> O (g) + Cr = MgO + CrCl <sub>2</sub> + H <sub>2</sub> (g)	–89.280 ✓
1.5MgCl <sub>2</sub> + 1.5H <sub>2</sub> O (g) + Cr = 1.5MgO + CrCl <sub>3</sub> + 1.5H <sub>2</sub> (g)	–70.398 ✓
2HCl (g) + Cr = CrCl <sub>2</sub> + H <sub>2</sub> (g)	–74.616 ✓
3HCl (g) + Cr = CrCl <sub>3</sub> + 1.5H <sub>2</sub> (g)	–48.403 ✓
MgCl <sub>2</sub> + H <sub>2</sub> O (g) + Ni = MgO + NiCl <sub>2</sub> + H <sub>2</sub> (g)	26.982
2.5MgCl <sub>2</sub> + 2.5H <sub>2</sub> O (g) + Mo = 2.5MgO + MoCl <sub>5</sub> + 2.5H <sub>2</sub> (g)	231.613
2HCl (g) + Ni = NiCl <sub>2</sub> + H <sub>2</sub> (g)	41.645
5HCl (g) + Mo = MoCl <sub>5</sub> + 2.5H <sub>2</sub> (g)	268.272
2CrCl <sub>2</sub> + 3H <sub>2</sub> O (g) + 2Ni = 2NiCl <sub>2</sub> + Cr <sub>2</sub> O <sub>3</sub> + 3H <sub>2</sub> (g)	–62.942 ✓
2CrCl <sub>3</sub> + 3H <sub>2</sub> O (g) + 3Ni = 3NiCl <sub>2</sub> + Cr <sub>2</sub> O <sub>3</sub> + 3H <sub>2</sub> (g)	–73.724 ✓
2CrCl <sub>2</sub> + 3H <sub>2</sub> O (g) + 1.333Mo = 1.333MoCl <sub>3</sub> + Cr <sub>2</sub> O <sub>3</sub> + 3H <sub>2</sub> (g)	–57.850 ✓
2CrCl <sub>3</sub> + 3H <sub>2</sub> O (g) + 2Mo = 2MoCl <sub>3</sub> + Cr <sub>2</sub> O <sub>3</sub> + 3H <sub>2</sub> (g)	–66.379 ✓
MgO + Cr <sub>2</sub> O <sub>3</sub> = MgCr <sub>2</sub> O <sub>4</sub>	–32.229 ✓
2CrCl <sub>3</sub> + 4MgO = MgCr <sub>2</sub> O <sub>4</sub> + 3MgCl <sub>2</sub>	–186.898 ✓

concentration of impurities and reduce the corrosiveness of molten NaCl–KCl–MgCl<sub>2</sub> salt. Besides, the salt chemistry of NaCl–KCl–MgCl<sub>2</sub> was changed through Mg treatment to reduce its corrosiveness [22]. Because there was no filtering of MgO from the molten salt, the generated MgO would deposit and accumulate on the alloy surface, forming a layer of MgO to inhibit further corrosion of 316 H SS in Fig. 12b. Therefore, Mg metal can effectively purify the molten NaCl–KCl–MgCl<sub>2</sub> salt, and the dissolved Mg metal (~0.025 wt%) used as the corrosion inhibitor to mitigate the corrosion of structural alloys. The corrosion rate of 316H SS in the purified NaCl–KCl–MgCl<sub>2</sub> salt was below 10 μm/year, which could meet the requirement of commercial applications (< 30 μm/year). Through the purification treatment of Mg metal, NaCl–KCl–MgCl<sub>2</sub> salt has the potential for engineering applications to MCFR reactors and CSP plants.

## 5 Conclusion

The corrosion behavior of 316H SS in the impure and purified NaCl–KCl–MgCl<sub>2</sub> salt at 700 °C was investigated to elaborate on the role of purification in mitigating the corrosiveness of NaCl–KCl–MgCl<sub>2</sub> salt. Results show that 316H SS suffered obvious weight loss and severe intergranular corrosion in the impure NaCl–KCl–MgCl<sub>2</sub> salt; the major metallic elements Fe, Cr, Ni, and Mo were depleted and diffused into molten salt. The corrosion depth of 316H SS was up to 130 μm for 1000 h. The strong corrosiveness of NaCl–KCl–MgCl<sub>2</sub> salt is attributed mainly to the absorbed H<sub>2</sub>O in the form of MgCl<sub>2</sub>·6H<sub>2</sub>O. This hydrated compound MgCl<sub>2</sub>·6H<sub>2</sub>O could decompose into hazardous impurities (H<sub>2</sub>O and HCl) at elevated temperatures and lead to the corrosion of 316H SS. Fortunately, the corrosiveness of the NaCl–KCl–MgCl<sub>2</sub> salt can be alleviated distinctly by the purification treatment with Mg metal. The Mg metal would act as the corrosion inhibitor to react with oxidizing impurities (H<sub>2</sub>O, HCl, metallic impurities) to reduce the corrosiveness of chloride salts. Experimental results confirmed that 316H SS exhibited excellent corrosion resistance in the purified NaCl–KCl–MgCl<sub>2</sub> salt, and the corrosion was attributed mainly to the dissolution of active Cr from the alloy matrix into molten salt. There was no obvious corrosion attack in the 316H SS. The corrosion rate of 316H SS in the purified NaCl–KCl–MgCl<sub>2</sub> salt was less than 10 μm/year, which is promising for its commercial application to the MCFR and CSP systems.

**Author contributions** All authors contributed to the study conception and design. Material preparation, data collection, and analysis were performed by Hua Ai, Xin-Mei Yang, and Yan-Jun Chen. The first draft of the manuscript was written by Hua Ai, and all authors commented on previous versions of the manuscript. All authors read and approved the final manuscript.

**Data availability** The data that support the findings of this study are openly available in Science Data Bank at <https://www.doi.org/10.57760/sciencedb.j00186.00331> and <https://cstr.cn/31253.11.sciencedb.j00186.00331>.

## Declarations

**Conflict of interest** The authors declare that they have no competing interests.

## References

1. R. Serrano-López, J. Fradera, S. Cuesta-López, Molten salts database for energy applications. *Chem. Eng. Process.* **73**, 87–102 (2013). <https://doi.org/10.1016/j.cep.2013.07.008>
2. M. Zhu, H. Yi, J. Lu et al., Corrosion of Ni–Fe based alloy in chloride molten salts for concentrating solar power containing aluminum as corrosion inhibitor. *Sol. Energ. Mat. Sol.* **241**, 111737 (2022). <https://doi.org/10.1016/j.solmat.2022.111737>
3. L.Y. He, S.P. Xia, X.M. Zhou et al., Th–U cycle performance analysis based on molten chloride salt and molten fluoride salt fast reactors. *Nucl. Sci. Tech.* **31**, 83 (2020). <https://doi.org/10.1007/s41365-020-00790-x>
4. L.Y. He, G.C. Li, S.P. Xia et al., Effect of <sup>37</sup>Cl enrichment on neutrons in a molten chloride salt fast reactor. *Nucl. Sci. Tech.* **31**, 27 (2020). <https://doi.org/10.1007/s41365-020-0740-x>
5. W. Ding, A. Bonk, T. Bauer, Molten chloride salts for next generation CSP plants: selection of promising chloride salts & study on corrosion of alloys in molten chloride salts. *AIP Conf. Proc.* **2126**, 200014 (2019). <https://doi.org/10.1063/1.5117729>
6. G. Mohan, M. Venkataraman, J. Gomez-Vidal et al., Assessment of a novel ternary eutectic chloride salt for next generation high-temperature sensible heat storage. *Energ. Convers. Manage.* **167**, 156–164 (2018). <https://doi.org/10.1016/j.enconman.2018.04.100>
7. X. Wei, M. Song, Q. Peng et al., A new ternary chloride eutectic mixture and its thermo-physical properties for solar thermal energy storage. *Energy Procedia.* **61**, 1314–1317 (2014). <https://doi.org/10.1016/j.egypro.2014.11.1089>
8. A.G. Fernández, M.I. Lasanta, F.J. Pérez, Molten salt corrosion of stainless steels and low-Cr steel in CSP plants. *Oxid. Met.* **78**, 329–348 (2012). <https://doi.org/10.1007/s11085-012-9310-x>
9. W. Ding, T. Bauer, Progress in research and development of molten chloride salt technology for next generation concentrated solar power plants. *Engineering* **7**, 334–347 (2021). <https://doi.org/10.1016/j.eng.2020.06.027>
10. B. Grégoire, C. Oskay, T.M. Meißner et al., Corrosion mechanisms of ferritic-martensitic P91 steel and Inconel 600 nickel-based alloy in molten chlorides. Part I: NaCl–KCl binary system. *Sol. Energ. Mat. Sol.* **215**, 110659 (2020). <https://doi.org/10.1016/j.solmat.2020.110659>
11. B. Grégoire, C. Oskay, T.M. Meißner et al., Corrosion mechanisms of ferritic-martensitic P91 steel and Inconel 600 nickel-based alloy in molten chlorides. Part II: NaCl–KCl–MgCl<sub>2</sub> ternary system. *Sol. Energ. Mat. Sol.* **216**, 110675 (2020). <https://doi.org/10.1016/j.solmat.2020.110675>
12. K. Vignarooban, P. Pugazhendhi, C. Tucker et al., Corrosion resistance of Hastelloys in molten metal-chloride heat-transfer fluids for concentrating solar power applications. *Sol. Energy* **103**, 62–69 (2014). <https://doi.org/10.1016/j.solener.2014.02.002>
13. W. Ding, H. Shi, Y. Xiu et al., Hot corrosion behavior of commercial alloys in thermal energy storage material of molten MgCl<sub>2</sub>/KCl/NaCl under inert atmosphere. *Sol. Energ. Mat. Sol.* **184**, 22–30 (2018). <https://doi.org/10.1016/j.solmat.2018.04.025>

14. M. Sarvghad, S. Delkassar Maher, D. Collard et al., Materials compatibility for the next generation of concentrated solar power plants. *Energy Storage Mater.* **14**, 179–198 (2018). <https://doi.org/10.1016/j.ensm.2018.02.023>
15. J.C. Gomez-Vidal, A.G. Fernandez, R. Tirawat et al., Corrosion resistance of alumina-forming alloys against molten chlorides for energy production. I. Pre-oxidation treatment and isothermal corrosion tests. *Sol. Energ. Mat. Sol.* **166**, 222–233 (2017). <https://doi.org/10.1016/j.solmat.2017.02.019>
16. H. Ai, S. Liu, X.X. Ye et al., Metallic impurities induced corrosion of a Ni-26W-6Cr alloy in molten fluoride salts at 850 °C. *Corros. Sci.* **178**, 109079 (2021). <https://doi.org/10.1016/j.corsci.2020.109079>
17. J. Qiu, B. Leng, H. Liu et al., Effect of  $\text{SO}_4^{2-}$  on the corrosion of 316L stainless steel in molten FLiNaK salt. *Corros. Sci.* **144**, 224–229 (2018). <https://doi.org/10.1016/j.corsci.2018.08.057>
18. S.S. Raiman, S. Lee, Aggregation and data analysis of corrosion studies in molten chloride and fluoride salts. *J. Nucl. Mater.* **511**, 523–535 (2018). <https://doi.org/10.1016/j.jnucmat.2018.07.036>
19. Q. Yang, J. Ge, J. Zhang, Electrochemical study on the kinetic properties of  $\text{Fe}^{2+}/\text{Fe}$ ,  $\text{Ni}^{2+}/\text{Ni}$ ,  $\text{Cr}^{2+}/\text{Cr}$  and  $\text{Cr}^{3+}/\text{Cr}^{2+}$  in molten  $\text{MgCl}_2$ -KCl-NaCl salts. *J. Electrochem. Soc.* **168**, 012504 (2021). <https://doi.org/10.1149/1945-7111/abdafa>
20. L. Guo, Q. Liu, H. Yin et al., Excellent corrosion resistance of 316 stainless steel in purified NaCl-MgCl<sub>2</sub> eutectic salt at high temperature. *Corros. Sci.* **166**, 012504 (2020). <https://doi.org/10.1016/j.corsci.2020.108473>
21. P. Lu, L. Guo, Q. Liu, et al., Excellent high temperature corrosion resistance of 304 stainless steel immersed in purified NaCl-MgCl<sub>2</sub> eutectic salts. *Mater. Chem. Phys.* **296** (2023). <https://doi.org/10.1016/j.matchemphys.2022.127216>
22. H. Sun, J.-Q. Wang, Z. Tang et al., Assessment of effects of Mg treatment on corrosivity of molten NaCl-KCl-MgCl<sub>2</sub> salt with Raman and Infrared spectra. *Corros. Sci.* **164**, 108350 (2019). <https://doi.org/10.1016/j.corsci.2019.108350>
23. W. Ding, J. Gomez-Vidal, A. Bonk et al., Molten chloride salts for next generation CSP plants: electrolytical salt purification for reducing corrosive impurity level. *Sol. Energ. Mat. Sol.* **199**, 8–15 (2019). <https://doi.org/10.1016/j.solmat.2019.04.021>
24. X.Q. Zheng, Q. Dou, M. Cheng et al., Study on removal of oxide from carrier salt in molten salt reactor by vacuum distillation. *Nucl. Tech.* **45**, 040302 (2022). <https://doi.org/10.11889/j.0253-3219.2022.hjs.45.040302>. (in Chinese)
25. J.W. Ambrosek, Molten chloride salts for heat transfer in nuclear systems. Dissertation, The University of Wisconsin, Madison (2011)
26. K. Hanson, K.M. Sankar, P.F. Weck et al., Effect of excess Mg to control corrosion in molten  $\text{MgCl}_2$  and KCl eutectic salt mixture. *Corros. Sci.* **194**, 109914 (2022). <https://doi.org/10.1016/j.corsci.2021.109914>
27. W. Ding, H. Shi, A. Jianu et al., Molten chloride salts for next generation concentrated solar power plants: mitigation strategies against corrosion of structural materials. *Sol. Energ. Mat. Sol.* **193**, 298–313 (2019). <https://doi.org/10.1016/j.solmat.2018.12.020>
28. S. Choi, N.E. Orabona, O.R. Dale et al., Effect of Mg dissolution on cyclic voltammetry and open circuit potentiometry of molten  $\text{MgCl}_2$ -KCl-NaCl candidate heat transfer fluid for concentrating solar power. *Sol. Energ. Mat. Sol.* **202**, 110087 (2019). <https://doi.org/10.1016/j.solmat.2019.110087>
29. A. Mortazavi, Y. Zhao, M. Esmaily, et al., High-temperature corrosion of a nickel-based alloy in a molten chloride environment—the effect of thermal and chemical purifications. *Sol. Energ. Mat. Sol.* **236**, 111542 (2022). <https://doi.org/10.1016/j.solmat.2021.111542>
30. X. Li, L. Chang, C. Liu et al., Effect of thermal aging on corrosion behavior of type 316H stainless steel in molten chloride salt. *Corros. Sci.* **191**, 109784 (2021). <https://doi.org/10.1016/j.corsci.2021.109784>
31. Q. Liu, H. Sun, H. Yin et al., Corrosion behaviour of 316H stainless steel in molten FLiNaK eutectic salt containing graphite particles. *Corros. Sci.* **160**, 108174 (2019). <https://doi.org/10.1016/j.corsci.2019.108174>
32. Q. Huang, G. Lu, J. Wang et al., Thermal decomposition mechanisms of  $\text{MgCl}_2 \cdot 6\text{H}_2\text{O}$  and  $\text{MgCl}_2 \cdot \text{H}_2\text{O}$ . *J. Anal. Appl. Pyrol.* **91**, 159–164 (2011). <https://doi.org/10.1016/j.jaap.2011.02.005>
33. Q. Liu, Z. Wang, W. Liu et al., Ni-Mo-Cr alloy corrosion in molten NaCl-KCl-MgCl<sub>2</sub> salt and vapour. *Corros. Sci.* **180**, 109183 (2021). <https://doi.org/10.1016/j.corsci.2020.109183>
34. W. Ding, A. Bonk, J. Gussone et al., Electrochemical measurement of corrosive impurities in molten chlorides for thermal energy storage. *J. Energy Storage* **15**, 408–414 (2018). <https://doi.org/10.1016/j.est.2017.12.007>
35. A. Plambeck, Electromotive force series in molten salts. *J. Chem. Eng. Data* **12**, 77–82 (1967). <https://doi.org/10.1021/je60032a023>

Springer Nature or its licensor (e.g. a society or other partner) holds exclusive rights to this article under a publishing agreement with the author(s) or other rightsholder(s); author self-archiving of the accepted manuscript version of this article is solely governed by the terms of such publishing agreement and applicable law.